JVST A
Journal of Vacuum Science & Technology A

ARTICLE

pubs.aip.org/avs/jva

Influence of atomic layer deposited Al_2O_3 thickness on metal/insulator/metal electron energy barriers

Cite as: J. Vac. Sci. Technol. A 44, 053210 (2026); doi: 10.1116/6.0005620
Submitted: 29 May 2026 · Accepted: 15 July 2026 ·
Published Online: 5 August 2026

Jessica Haglund and John F. Conley, Jr.[a)]

AFFILIATIONS

School of Electrical Engineering and Computer Science, Oregon State University, Corvallis, Oregon 97331

[a)]**Author to whom correspondence should be addressed:** jconley@eecs.oregonstate.edu

ABSTRACT

It has been reported that the relative dielectric constant, refractive index, and density of certain thin dielectric films, such as Al_2O_3, degrade with decreasing thickness. We investigated the influence of Al_2O_3 film thickness on the electron energy barriers at the interfaces of Pt/Al_2O_3/TiN metal/insulator/metal devices with Al_2O_3 deposited via atomic layer deposition. Using internal photoemission spectroscopy, we found that both the top Pt/Al_2O_3 and bottom TiN/Al_2O_3 electron barriers were a function of Al_2O_3 thickness. While both electron barriers were roughly constant at ~3.6 eV for films ≥11.6 nm thick, both decreased by ~0.5 eV as Al_2O_3 thickness decreased to 4.5 nm. The degradation of electron barriers with insulator thickness impacts the modeling of leakage currents and optimization of performance in devices with ultrathin insulators.

I. INTRODUCTION

Ultrathin dielectrics find wide use in metal/insulator/metal (MIM) capacitors, high speed MIM tunnel diodes, metal/oxide/semiconductor (MOS) transistor gates, and Si qubits. The properties of ultrathin insulating films are often a function of thickness, typically degrading as films become thinner. An early report by Birey *et al.* showed that the dielectric constant, κ, of evaporated Al_2O_3 decreased from a bulklike κ = 9 for 100 nm thick films to κ = 7 for 20 nm films and further decreased to κ ~ 4.5 for 6 nm films.[1] They proposed that the rapid decrease in κ below 20 nm was due to structural discontinuities in the film. A similar degradation in κ with decreasing thickness was reported by Groner *et al.* for atomic layer deposited (ALD) Al_2O_3 on both thin Mo films and Si substrates, with κ = 7.6 for 115 nm thick Al_2O_3 films decreasing to κ = 4 for 3 nm films.[2] Etinger-Geller *et al.* later showed that the optical refractive index of ALD Al_2O_3 also decreased with thickness, from $n = 1.63$ for a 64 nm film to ~1.60 for a 17 nm thick film,[3] and that the density of ALD Al_2O_3 films deposited at 200 °C decreased gradually from 3.4 g/cm^3 at 40 nm to 2.6 g/cm^3 at 15 nm. They also noted that films deposited at 300 °C remained at 3.4 g/cm^3 down to a thickness of 25 nm before steeply decreasing to 2.6 g/cm^3 at ~15 nm.[4] Groner *et al.* had previously reported that the density of Al_2O_3 films decreased steadily with decreasing deposition temperature from ~3.0 g/cm^3 at 172 °C to 2.5 g/cm^3 at room temperature.[5] Together, these studies suggest that the quality of the initial layers of an ALD film may be similar to thicker films deposited at lower temperatures. Work on other ALD films has also shown thickness dependencies. Kim *et al.* showed that the phase of ALD TiO_2 deposited at 250 °C shifts from amorphous to crystalline above a critical thickness of ~11 nm.[6] The transition was not observed for depositions at 235 °C, and the critical thickness was shifted down to ~8 nm at 260 °C. A decrease in the refractive index with decreasing thickness was reported for ALD TiO_2 and was attributed to either reduced density or reduced crystallinity.[7] For ALD ZnO, a reduction in the high frequency dielectric constant and a change in IR absorption were reported as thickness decreased from 20 to 5 nm.[8] It has also been shown that in ALD nanolaminates with a fixed composition and total thickness, the thickness of the bilayers had a strong influence on electrical properties.[9]

Despite all these reports of thickness dependent properties, there has been no direct and systematic assessment of the impact of insulator thickness on the electron energy barriers in functional electronic devices with metal electrodes. Knowledge of these

barriers is critical in predicting and optimizing electrical performance, threshold voltage, and leakage of MIM and MOS devices, such as Si qubits.[10,11] Although capacitance versus voltage (CV) measurements of flatband voltage can be used to estimate the effective work function of metals in MOS structures, this method requires an array of insulator thicknesses and the assumption that the properties of the insulator do not vary with thickness. The only technique that allows for direct barrier height determination in a fully formed device under active operation is internal photoemission (IPE) spectroscopy. IPE is an optical electrical method in which spectral thresholds, φ_{thresh}, for electron emission are taken at a range of electric fields and used to extrapolate the barrier height at zero applied field, φ_{Bn}.[12–19]

In this work, IPE spectroscopy was used to determine the impact of ALD Al_2O_3 film thickness on electron energy barriers at both the top and bottom interfaces of Pt/Al_2O_3/TiN MIM devices. It was found that φ_{Bn} at both interfaces degraded with decreasing Al_2O_3 thickness below 12 nm, an important consideration for estimating leakage in device technologies employing thin insulators.

II. EXPERIMENTAL DETAILS

For the first set of devices, Al_2O_3 was deposited via ALD in a Picosun R-150 reactor at 250 °C using 0.1 s pulses of trimethylaluminum [$Al(CH_3)_3$, TMA] and H_2O separated by 10 s N_2 purges. The growth per cycle was determined to be 0.9 nm/cycle. An array of samples with Al_2O_3 thicknesses ($d_{Al_2O_3}$) of 4.5, 6.8, 8.7, 11.6, 16.7, and 18.0 nm were created by varying the number of ALD cycles (50, 75, 100, 125, 175, and 200 cycles, respectively). The Al_2O_3 film thickness was measured across Si witness coupons using a Film Sense FS-1 multiwavelength mapping ellipsometer and modeled using a Cauchy model on Si with a native oxide. The native oxide thickness was measured prior to deposition. Following Al_2O_3 deposition on 100 nm thick sputtered TiN blanket bottom electrodes, MIM devices were completed by forming 10 nm thick semitransparent Pt top electrodes by electron beam deposition through a shadow mask, resulting in 50, 125, 250, and 500 μm diameter circular devices. A schematic cross section is shown as an inset in Fig. 1.

In a second set of devices, the Al_2O_3 thickness array was repeated, wherein a 1 nm thick Ti adhesion layer was electron beam deposited prior to Pt deposition. A third set of devices had a sputtered blanket bottom Pt electrode purchased from LGA Thin Films (Santa Clara) with 10 nm ALD Al_2O_3 deposited in a Picosun R-200 reactor at 250 °C.

CV measurements were performed on 125 and 250 μm diameter devices at 100 kHz and an AC signal amplitude of 25 mV on an Agilent 4284A using a probe station in a dark box and corrected for parallel resistance. Bias was applied to the Pt top electrode while the TiN bottom electrode was held at ground.

IPE measurements were performed on 250 and 500 μm diameter devices using a lab built system described previously.[12,18,20] Briefly, light from a 150 W Xe arc lamp was passed through a Princeton Instrument SP2150i monochromator and then through bandpass filters before being focused with a mirror onto the top electrode of the MIM devices. Fresh devices were used for top and bottom barrier measurements. To measure IPE from the top

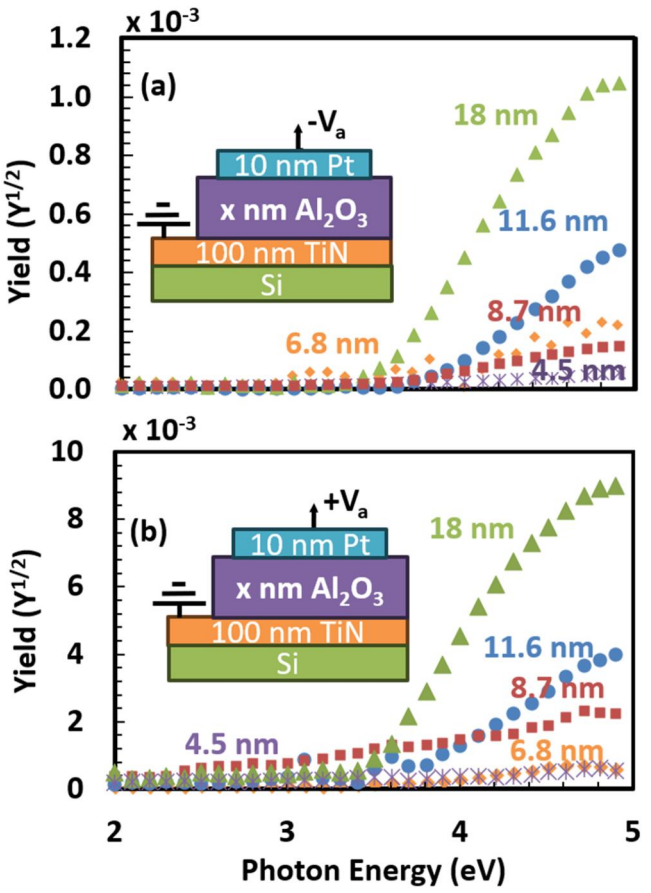

FIG. 1. Representative IPE yield plots for Pt/Al_2O_3/TiN MIM devices with various $d_{Al_2O_3}$ (* 4.5 nm, ◇ 6.8 nm, ■ 8.7 nm, ● 11.6 nm, ▲18.0 nm) for (a) negative polarity ($\xi_{Al_2O_3} = -1$ MV/cm) and (b) positive polarity ($\xi_{Al_2O_3} = +1$ MV/cm).

(bottom) electrode, voltage was stepped from 0 to −2 V (0 to +2 V) in −0.1 V (+0.1 V) increments using a Yokogawa GS200 DC voltage source. For each applied bias, the average dark current, I_{dark}, was first determined by taking a 30 s average with no light. Then, the photon energy, E_{ph}, was swept from 1.7 to 5.5 eV in 0.1 eV steps and the average current, I_{IPE}, was measured at each E_{ph}. Current was measured using a Keithley 617 electrometer unless otherwise noted. The IPE quantum yield, Y, at each photon energy was taken as $Y = (I_{IPE} - I_{\text{dark}}) * E_{ph}/P_{\text{lamp}}(E_{ph})$, where $P_{\text{lamp}}(E_{ph})$ is the power of the lamp at each photon energy. The spectral onset threshold, φ_{thresh}, of IPE at each field was determined using a linear extrapolation to the x axis of a plot of $Y^{1/2}$ (for emission from a metal)[13,21] versus E_{ph}. An algorithm was used to find the largest region of the $Y^{1/2}$ curve with the highest linearity, as determined from the R^2 value of a linear regression.[18,20] The electric field across Al_2O_3, $\xi_{Al_2O_3}$, was determined by subtracting built-in voltage across Al_2O_3 due to the electrode effective work function difference, V_{bi}, from each applied voltage and

then dividing by the Al_2O_3 thickness. V_{bi} was determined as the applied voltage at which the I_{dark} switches from negative to positive. φ_{thresh} values were then plotted versus $|\xi_{Al_2O_3}^{1/2}|$, and a linear fit was used to extrapolate zero field ($\xi_{Al_2O_3} = 0$) electron barrier heights, φ_{Bn}, defined as the distance from the Fermi level of the respective metal gate to the conduction band edge of Al_2O_3. IPE φ_{Bn} estimation error is roughly ±0.1 eV for comparing different devices and less than ±0.03 eV for repeated measurements on the same device (see Fig. S1 in the supplementary material).

III. EXPERIMENTAL RESULTS

Shown in Fig. 1(a) are the representative yield plots for $\xi_{Al_2O_3} = -1$ MV/cm (IPE from the Pt top electrode) for Pt/Al_2O_3/TiN MIM devices with several different thicknesses of Al_2O_3. The devices with $d_{Al_2O_3} = 18$ nm showed both a steep φ_{thresh} transition from a flat baseline and the highest yield, while devices with thinner Al_2O_3 showed shallower φ_{thresh} transitions and apparent reductions in the yield. Normalized yield plots [see Fig. S2(a) in the supplementary material] revealed that devices with thinner Al_2O_3 showed increased noise and apparent increases in baseline and tailing (stretch-out of the yield curve to lower energies), all of which became worse with decreasing $d_{Al_2O_3}$. As discussed in the supplementary material, the increased noise and apparent increases in baseline and tailing were all correlated with increases in I_{dark} (see Fig. S3 in the supplementary material) and were measurement artifacts of the electrometer. Though responsible for the apparent decreases in the yield in Fig. 2(a), these artifacts did not impact the extraction of φ_{thresh} values.

Shown in Fig. 1(b) are the representative yield curves for $\xi_{Al_2O_3} = +1$ MV/cm (IPE from the TiN bottom electrode). The devices with 20 nm Al_2O_3 again showed a steep φ_{thresh} from a flat baseline and the highest absolute yield. Normalized plots [Fig. S2 (b) in the supplementary material] indicated that the devices with thinner Al_2O_3 layers showed the same trends as seen for the top electrode: increased noise, apparent increased baseline, more evident tailing, and reduced yield magnitude also due to increased leakage (I_{dark}), as mentioned above.

Figure 2 shows the Schottky plots for the top and bottom electrodes from which the zero field barrier heights, $\varphi_{Bn,Pt/Al_2O_3}$ and $\varphi_{Bn,TiN/Al_2O_3}$, were extrapolated. Data on the 6.8 nm devices were taken with a Keithley 6517 electrometer (see Fig. S4 for discussion). φ_{Bn} values are summarized in Table I and plotted versus $d_{Al_2O_3}$ in Fig. 3. Both the top Pt/Al_2O_3 and bottom TiN/Al_2O_3 electron barriers were found to be a function of Al_2O_3 thickness. While $d_{Al_2O_3} \geq 11.8$ nm, both barriers remained constant within experimental error at approximately 3.6 eV. For $d_{Al_2O_3} < 11.6$ nm, both $\varphi_{Bn,Pt/Al_2O_3}$ and $\varphi_{Bn,TiN/Al_2O_3}$ decreased, and at $d_{Al_2O_3} = 4.5$ nm, were 3.2 and 3.1 eV, respectively.

Shown in Fig. 4 is a plot of the relative dielectric constant, κ, versus $d_{Al_2O_3}$ for the Pt/Al_2O_3/TiN MIM devices. κ values were determined from the slope of the zero oxide field capacitance, C_0, of MIM C-V measurements using two device areas. MIM C-V curves showed the very slightly positive parabolic curvature typical of Al_2O_3, described by the following equation:

$$C(V) = C_0\left(1 + \alpha_{VCC}V + \beta_{VCC}V^2\right), \quad (1)$$

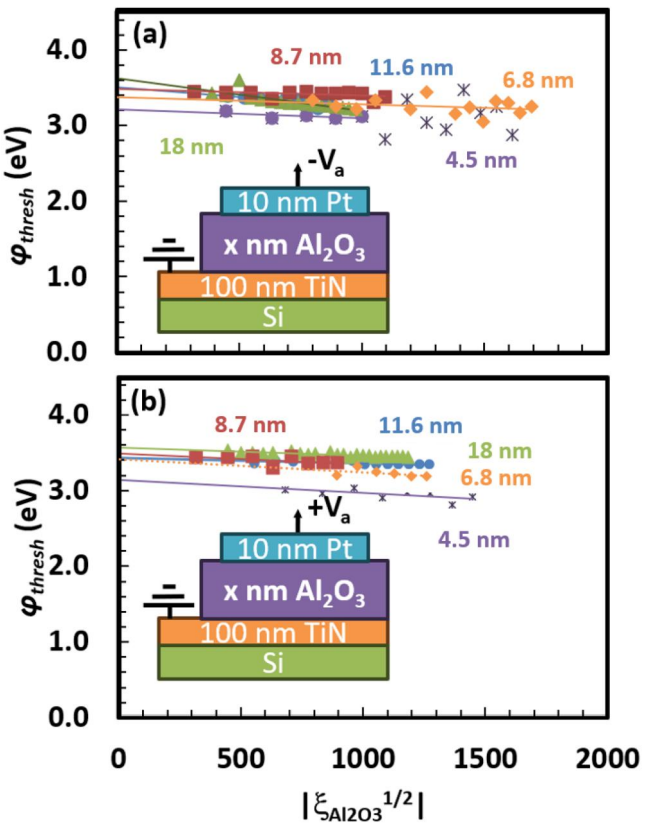

FIG. 2. Schottky plots of φ_{thresh} vs $|\xi_{Al_2O_3}^{1/2}|$ for Pt/Al_2O_3/TiN MIM devices with various d_{Al2O3} (* 4.5 nm, ◇ 6.8 nm, ■ 8.7 nm, ● 11.6 nm, ▲18.0 nm) under (a) negative and (b) positive polarity. Lines show the data used for extrapolation. Error bars are less than the size of the symbols.

where α_{VCC} and β_{VCC} are the quadratic and linear coefficients of capacitance, respectively.[22] At $d_{Al_2O_3} \geq 16.8$ nm, κ appeared saturated at 8.7, matching well with literature values for ALD Al_2O_3 deposited using TMA and H_2O.[23] At $d_{Al_2O_3} \leq 11.6$ nm, κ decreased with decreasing d_{Al2O3}, consistent with previous reports on MOS devices.[2,3]

IV. DISCUSSION

The 0.4 and 0.5 eV reduction, respectively, of the top and bottom electron barriers with decreasing Al_2O_3 thickness (Fig. 3)

TABLE I. Summary of $\varphi_{Bn,Pt/Al_2O_3}$ and $\varphi_{Bn,TiN/Al_2O_3}$ for various $d_{Al_2O_3}$.

$d_{Al_2O_3}$ (nm)	$\varphi_{Bn,Pt/Al_2O_3}$ (eV)	$\varphi_{Bn,TiN/Al_2O_3}$ (eV)
4.5	3.22 (3)	3.13 (3)
6.8	3.40 (3)	3.45 (3)
8.7	3.47 (3)	3.49 (3)
11.6	3.56 (3)	3.60 (3)
16.8	3.60 (3)	3.55 (3)
18.0	3.63 (3)	3.60 (3)

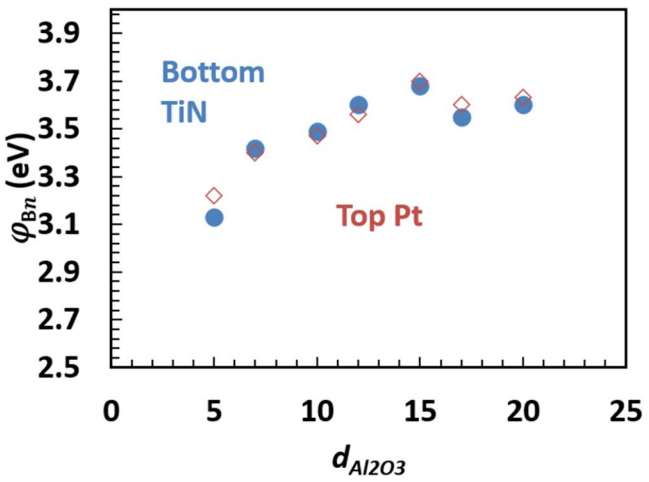

FIG. 3. Plot of φ_{Bn} vs $d_{Al_2O_3}$ for the top Pt (◇) and bottom TiN (●) interfaces of $Pt/Al_2O_3/TiN$ MIM devices. Error bars are less than the size of the symbols.

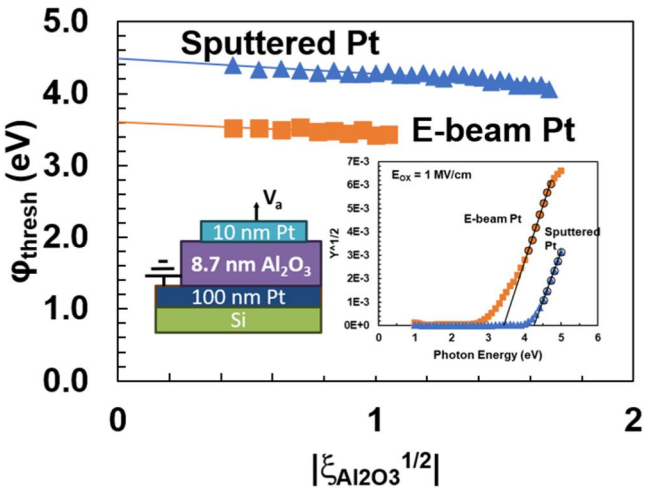

FIG. 5. IPE Schottky plots for emission from the top e-beam Pt and bottom sputtered Pt electrode in $Pt/Al_2O_3/Pt$ MIM devices. The inset on the left shows the device schematic cross section, and the inset on the right shows the representative IPE yield plots for top (−1 MV/cm, ■) and bottom (1 MV/cm, ▲) electrodes. Error bars are less than the size of the symbols.

was consistent with the reduction in κ seen in Fig. 4. This demonstrates that, along with previous reports of κ, film density, and optical refractive index,[2–4] interfacial energy barriers also degrade with decreasing Al_2O_3 thickness.

From Fig. 3 and Table I, it is seen that the Pt and TiN barriers are roughly equal within experimental error. Based on relative vacuum work functions, sputtered TiN ($\Phi_{TiN,vac} = 4.4–4.8$ eV, strongly dependent on processing)[24,25] would typically be expected to have a smaller barrier than Pt ($\Phi_{Pt,vac} \sim 5.6$ eV)[26] The measured $\varphi_{Bn,TiN/Al_2O_3}$ is consistent with previous IPE reports, which range from 3.0 to 3.8 eV for sputtered TiN.[27–29]

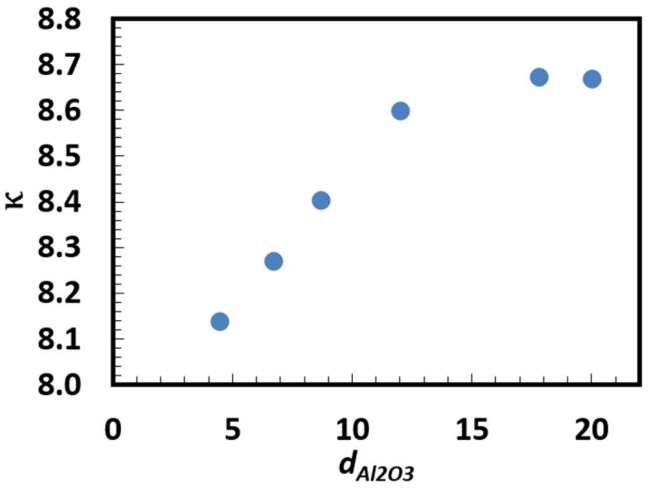

FIG. 4. Plot of κ vs $d_{Al_2O_3}$ for the $Pt/Al_2O_3/TiN$ MIM devices.

The measured $\varphi_{Bn,Pt/Al_2O_3}$ is near the low end of the 3.7–4.6 eV range calculated from the difference between $\Phi_{Pt,vac}$ and $\chi_{Al_2O_3}$ ($\chi_{Al_2O_3} = 1.0–1.9$ eV).[30–32] The only other IPE φ_{Bn} study of a direct Pt/Al_2O_3 interface (with sputtered Pt and 19 nm thick ALD Al_2O_3) reported φ_{Bn} values of either 3.3 or 2.9 eV, followed by 400 °C anneals in either vacuum or H_2, respectively.[33] Both of these values are much lower than what we see for the 18 nm Al_2O_3, and well outside of the Schottky–Mott prediction range, but close to what we found for 4.5 nm Al_2O_3 devices. As an additional comparison, shown in Fig. 5, are the IPE Schottky plots for nominally symmetric $Pt/Al_2O_3/Pt$ devices with the same electron beam deposited Pt top gate used in this study but with 100 nm sputtered Pt as the bottom electrode. The extrapolated zero field barriers for electron beam (top) and sputtered Pt (bottom) were 3.61(3) and 4.48(3) eV, respectively. The top electron beam Pt barrier was within the error of that measured on the $Pt/Al_2O_3/TiN$ devices (Table I). The sputtered bottom Pt barrier was more than 0.8 eV larger and was near the top end of the Schottky–Mott prediction ($\Phi_{Pt,vac} - \chi_{Al_2O_3}$) range. The different barrier heights observed among the various Pt/Al_2O_3 interfaces in the present and previous report illustrate the need for measuring barriers in specific stacks and may be attributed to the different deposition methods and processing. For example, as postulated by Kolomiiets *et al.*,[33] the ~0.9 eV lower barrier seen for the top electron beam Pt might have been due to the process induced interfacial dipole. Note that increased thickness of a single layer Pt electrode above roughly 1 nm is unlikely to have a strong direct influence on barrier height.[34] Metal thickness might be expected to play a secondary role, however, potentially influencing IPE measurements through physical parameters such as strain mismatch and grain size.[35] A 0.2 eV difference in IPE top versus bottom electrode

barriers has also been reported for a nominally symmetric TiN/Al_2O_3/TiN structure.[29]

To achieve good adhesion of Pt to insulators, thin wetting layers such as Ti are typically used. In a previous IPE study of the impact of Ti adhesion layer thickness on the electron barriers of Pt/Ti/Al_2O_3/TiN devices, it was found that, in the absence of diffusion from a metal capping/overlayer, even a ~1 nm layer of interfacial Ti was sufficient to set the barrier.[34] Toward extending the observation of the impact of Al_2O_3 thickness on $\varphi_{Bn's}$ to an additional metal, Al_2O_3 thickness arrays in which the Pt top gate had Ti adhesion layers of 1 or 10 nm were also investigated. However, it was found that I_{dark} increased much more steeply with decreasing d_{Al2O3} in the Pt/Ti/Al_2O_3 arrays than in the direct Pt/Al_2O_3 device arrays so that yield curves for devices with $d_{Al2O3} \leq 10$ nm were dominated by noise, making it impossible to extract accurate φ_{Bn}'s. The increased leakage was likely due to the scavenging of oxygen by the Ti interfacial layer and the creation of oxygen vacancies in Al_2O_3.[36,37]

V. SUMMARY AND CONCLUSIONS

In summary, the impact of ALD Al_2O_3 thickness on interfacial electron energy barriers in Pt/Al_2O_3/TiN MIM devices was measured for the first time by IPE spectroscopy. It was found that both top and bottom electron energy barriers were a function of $d_{Al_2O_3}$. For $d_{Al_2O_3} \geq 11.6$ nm, $\varphi_{Bn,Pt/Al_2O_3}$ and $\varphi_{Bn,TiN/Al_2O_3}$ were independent of Al_2O_3 thickness, saturating at roughly 3.6 eV. Below 11.6 nm, both $\varphi_{Bn,Pt/Al_2O_3}$ and $\varphi_{Bn,TiN/Al_2O_3}$ degraded steadily with thickness and at 4.5 nm were 3.2 and 3.1 eV, respectively. It was confirmed with CV measurements that κ also decreased as Al_2O_3 thickness was reduced below 11.6 nm, from 8.7 at $d_{Al_2O_3} \geq 17$ nm to 8.1 at 4.5 nm, consistent with previous reports.[2] The 0.4 and 0.5 eV reduction of the bottom and top electron barriers, respectively, observed in this work demonstrates that not only κ, density, and refractive index,[3,4] but also interfacial energy barriers degrade with decreasing Al_2O_3 thickness.

Ultrathin dielectrics are widely used in MOS gate dielectrics, MIM capacitors, high speed MIM tunnel diodes, and Si qubits. The dependence of barrier height on thickness will need to be considered when modeling tunneling currents in these devices. The results presented here provide further evidence that sub-10 nm ALD Al_2O_3 films are of lower quality, which, based on previous reports,[2–5,7] we infer may be due to incomplete formation during the initial nucleation, poor stoichiometry, decreased density, and increased defect/impurity incorporation. This is likely to extend to other ALD films as well. The similarity of ultrathin film properties to films deposited at lower temperatures suggests that advanced methods such as energy enhanced ALD may be needed to improve ALD nucleation and growth.[5,38–41]

SUPPLEMENTARY MATERIAL

See the supplementary material for figures and discussions referred to in the paper.

ACKNOWLEDGMENTS

The authors acknowledge the Air Force Office of Scientific Research for financial support of this project through the Department of Energy and Sandia National Labs. This work was performed at the Materials Synthesis and Characterization (MaSC) Center, a National Science Foundation (NSF) National Nanotechnology Coordinated Infrastructure (NNCI) Northwest Nanotechnology Infrastructure (NWNI) open user facility at Oregon State University, supported, in part, through NSF Grant No. NNCI-2025489. The authors also thank Shashank Misra and Christopher Allemang for their discussions regarding qubit operation and optimization.

AUTHOR DECLARATIONS

Conflict of Interest

The authors have no conflicts to disclose.

Author Contributions

Jessica Haglund: Investigation (equal); Writing – original draft (equal); Writing – review & editing (equal). **John F. Conley, Jr.:** Conceptualization (equal); Funding acquisition (equal); Writing – original draft (equal); Writing – review & editing (equal).

DATA AVAILABILITY

The data that support the findings of this study are available from the corresponding author upon reasonable request.

REFERENCES

[1]H. Birey, J. Appl. Phys. **48**, 5209 (1977).
[2]M. D. Groner, J. W. Elam, F. H. Fabreguette, and S. M. George, Thin Solid Films **413**, 186 (2002).
[3]Y. Etinger-Geller, E. Zoubenko, M. Baskin, L. Kornblum, and B. Pokroy, J. Appl. Phys. **125**, 185302 (2019).
[4]Y. Etinger-Geller, A. Katsman, and B. Pokroy, Chem. Mater. **29**, 4912 (2017).
[5]M. D. Groner, F. H. Fabreguette, J. W. Elam, and S. M. George, Chem. Mater. **16**, 639 (2004).
[6]S. K. Kim, S. Hoffmann-Eifert, M. Reiners, and R. Waser, J. Electrochem. Soc. **158**, D6 (2011).
[7]R. L. Wilson, C. E. Simion, B. S. Christopher, C. J. Carmalt, A. Stanoiu, F. Di Maggio, and J. A. Covington, Sensors **18**, 735 (2018).
[8]N. S. Samarasingha, S. Zollner, D. Pal, R. Singh, and S. Chattopadhyay, J. Vac. Sci. Technol. B **38**, 042201 (2020).
[9]S. W. Smith, K. G. McAuliffe, and J. F. Conley, Jr., Solid-State Electron. **54**, 1076 (2010).
[10]S. J. Angus, A. J. Ferguson, A. S. Dzurak, and R. G. Clark, Nano Lett. **7**, 2051 (2007).
[11]G. J. Podd, S. J. Angus, D. A. Williams, and A. J. Ferguson, Appl. Phys. Lett. **96**, 082104 (2010).
[12]J. Haglund, T. Mimura, J. F. Ihlefeld, and J. F. Conley, Jr., ACS Appl. Electron. Mater. **6**, 3249 (2024).
[13]V. K. Adamchuk and V. V. Afanas'ev, Prog. Surf. Sci. **41**, 111 (1992).
[14]V. V. Afanas'ev and A. Stesmans, J. Appl. Phys. **102**, 081301 (2007).
[15]N. V. Nguyen *et al.*, AIP Conf. Proc. **931**, 308 (2007).
[16]V. V. Afanas'ev *et al.*, Appl. Phys. Lett. **98**, 132901 (2011).
[17]N. V. Nguyen, O. A. Kirillov, and J. S. Suehle, Thin Solid Films **519**, 2811 (2011).
[18]M. A. Jenkins, T. Klarr, D. Z. Austin, W. Li, N. V. Nguyen, and J. F. Conley, Jr., Phys. Status Solidi RRL **12**, 1700437 (2018).
[19]M. A. Jenkins *et al.*, ACS Appl. Mater. Interfaces **13**, 14634 (2021).

[20]M. A. Jenkins, J. M. McGlone, J. F. Wager, and J. F. Conley, Jr., J. Appl. Phys. **125**, 055301 (2019).
[21]V. V. Afanas'ev, "Silicon–insulator interface barriers," in *Internal Photoemission Spectroscopy*, 2nd ed., edited by V. V. Afanas'ev (Elsevier, Oxford, 2014), pp. 255–299.
[22]D. Z. Austin, K. E. K. Holden, J. Hinz, and J. F. Conley, Jr, Appl. Phys. Lett. **110**, 263503 (2017).
[23]J. Acharya, J. Wilt, B. Liu, and J. Wu, ACS Appl. Mater. Interfaces **10**, 3112 (2018).
[24]Y. Zhuang, Y. Liu, H. Xia, Y. Li, X. Li, and T. Li, AIP Adv. **12**, 125222 (2022).
[25]Y. Liu *et al.*, IEEE Trans. Nanotechnol. **5**, 723 (2006).
[26]H. B. Michaelson, J. Appl. Phys. **48**, 4729 (1977).
[27]K. E. K. Holden, Y. Qi, and J. F. Conley, Jr., J. Appl. Phys. **129**, 144502 (2021).
[28]F. De Stefano, V. V. Afanas'ev, M. Houssa, L. Goux, K. Opsomer, M. Jurczak, and A. Stesmans, Phys. Status Solidi A **211**, 382 (2014).
[29]V. Afanas'ev, N. Kolomiiets, M. Houssa, and A. Stesmans, Phys. Status Solidi A **215**, 1700865 (2018).
[30]F. De Stefano, V. V. Afanas'ev, M. Houssa, A. Stesmans, K. Opsomer, M. Jurczak, and L. Goux, Microelectron. Eng. **109**, 156 (2013).
[31]J. Robertson, J. Vac. Sci. Technol B **18**, 1785 (2000).
[32]R. Ludeke, M. T. Cuberes, and E. Cartier, Appl. Phys. Lett. **76**, 2886 (2000).
[33]N. M. Kolomiiets, V. V. Afanas'ev, K. Opsomer, M. Houssa, and A. Stesmans, Phys. Status Solidi A **213**, 260 (2016).
[34]J. Haglund and J. F. Conley, Jr., J. Appl. Phys. **139**, 245303 (2026).
[35]R. M. Stein, Z. S. Barcikowski, S. J. Pookpanratana, J. M. Pomeroy, and M. D. Stewart, Jr., J. Appl. Phys. **130**, 115102 (2021).
[36]E. O. Filatova, A. S. Konashuk, S. S. Sakhonenkov, A. A. Sokolov, and V. V. Afanas'ev, Sci. Rep. **7**, 4541 (2017).
[37]S. Fadida, L. Nyns, S. Van Elshocht, and M. Eizenberg, J. Electron. Mater. **46**, 386 (2017).
[38]J. F. Conley, Jr., Y. Ono, and D. J. Tweet, Appl. Phys. Lett. **84**, 1913 (2004).
[39]W.-H. Lee, W.-C. Kao, Y.-T. Yin, S.-H. Yi, K.-W. Huang, H.-C. Lin, and M.-J. Chen, Appl. Surf. Sci. **525**, 146615 (2020).
[40]S. T. Ueda *et al.*, J. Mater. Chem. C **10**, 5707 (2022).
[41]B. Kupp, J. Haglund, S. Witsell, M. Kamarehi, and J. F. Conley, Jr., J. Vac. Sci. Technol. A **43**, 052403 (2025).